

The Mott State and Superconductivity in Face-Centred Cubic Structured Cs₃C₆₀: A ¹³³Cs-Nuclear Magnetic Resonance Study under Pressure

Shinji Kawasaki¹, Junji Fukui¹, Takeshi Motoyama¹, Yuta Suzuki¹, Seiji Shibusaki¹, and Guo-qing Zheng^{1,2}

¹*Department of Physics, Faculty of Science, Okayama University, Okayama 700-8530, Japan and*

³*Institute of Physics and Beijing National Laboratory for Condensed Matter Physics, Chinese Academy of Sciences, Beijing 100190, China*

Over the past 20 years, fullerenes have been studied as the source of high-transition-temperature (T_c) superconductivity except for copper oxides. The recent finding of the Mott insulating state right beside superconductivity in Cs₃C₆₀ has suggested that magnetism helps raise T_c even in fullerenes as in heavy-fermion compounds, high- T_c copper oxides, two-dimensional organic conductors, and iron pnictides. Namely, one tends to think that the link between Mott insulator and superconductivity takes place in fullerenes, which can give rise to the mechanism beyond the Bardeen-Cooper-Schrieffer framework. However, the relationship between the Mott state and the superconductivity in Cs₃C₆₀ is still under debate. By nuclear magnetic resonance measurements under pressure, we find that the magnetism and superconductivity in Cs₃C₆₀ are competing orders. Different from previous reports, the phase separation of Cs₃C₆₀ crystals into the Mott and metallic states allows us to systematically study the evolution of the ground state under pressure. Our careful experiments have found that the prevention of a magnetic order is rather essential for the superconductivity in face-centred cubic Cs₃C₆₀, which presents a basic strategy for finding still higher T_c in this system.

I. INTRODUCTION

The alkali-doped fullerenes A_3C_{60} (A : alkali ion) have been studied as the source of high-transition-temperature (T_c) superconductivity¹. The highest T_c of 38 K has been reported in the A15 phase of Cs₃C₆₀ under pressure²⁻⁴. The reported superconducting dome beside a Mott insulating phase²⁻⁴ is similar to that in heavy-fermion compounds⁵, high T_c copper oxides⁶, two-dimensional organic conductors^{7,8}, and iron pnictides^{9,10}. Furthermore, the coexistence of antiferromagnetism and superconductivity has been suggested³. In order for superconductivity to survive and even to be enhanced in the vicinity of a Mott state, new mechanisms beyond the Bardeen-Cooper-Schrieffer (BCS) framework have been expected^{1-4,11-13}.

Among its polymorphism, the face-centred-cubic (fcc) A_3C_{60} also shows high- T_c superconductivity. Its T_c increases with increasing lattice constant by replacing the A with a larger alkali ion¹⁴⁻¹⁶. Replacing the alkali ion K with Rb significantly increases T_c from 20 to 30 K¹⁵. Furthermore, replacing Rb with Cs resulted in $T_c = 31.3$ K for Rb₂CsC₆₀¹⁵ and in $T_c = 33$ K for RbCs₂C₆₀¹⁶. This relationship between T_c and the lattice parameter suggests that the superconductivity is due to a conventional electron-phonon interaction because the decrease in the extent of overlapping of the molecular wave function drives the density of states, $N(E_F)$, up, and thus T_c increases^{17,18}. However, since the large C₆₀-C₆₀ distance causes the localization of electrons on C₆₀ balls, the end member of fcc Cs₃C₆₀ becomes a Mott insulator with $T_N \sim 2.5$ K⁴. T_N is one order of magnitude smaller and the observed internal magnetic field is much smaller than those of A15 Cs₃C₆₀ owing to geometrical spin frustration²⁻⁴. Notably, the highest T_c of 35 K among fcc A_3C_{60} 's is found after suppressing this Mott state under pressure⁴. Thus, whether the metal-insulator

transition plays any role in inducing high- T_c superconductivity has become an issue in fullerenes^{1-4,11-13}. The previous nuclear magnetic resonance (NMR) experiment suggested that the end point of metal-insulator transition exists above the superconducting dome, indicating that the electronic correlations leading to the Mott state also play a role in having a maximal T_c adjacent to the Mott phase in Cs₃C₆₀ under pressure¹³.

In this paper, we report that the Mott state and superconductivity of fcc Cs₃C₆₀ are competing orders. Our careful ¹³³Cs-NMR spectrum and nuclear spin-lattice-relaxation time (T_1) measurements revealed that there are two different electronic phases for fcc Cs₃C₆₀. We find that the Mott state is robust against pressure and that the pressure-temperature phase diagram reported thus far^{2,4,13} is difficult to understand only by the pressure effect on the Mott state. The other seed for superconductivity, namely, paramagnetic metal, is hidden in the background of the Mott state, which realizes the phase separation of the two orders of antiferromagnetism and superconductivity in the low-pressure region. For comparison, with a previous structural study under pressure⁴, we present a new phase diagram of temperature versus unit-cell volume around the Mott insulator-to-metal transition, which unambiguously indicates that the Mott state is unfavourable for forming Cooper pairs in Cs₃C₆₀.

II. EXPERIMENTAL PROCEDURE

fcc Cs₃C₆₀ crystals were synthesized by a solution process with CH₃NH₂ at low temperatures². Nominal amounts of Cs and C₆₀ were introduced into glass tubes in an Ar glove box (O₂ < 0.1 ppm and H₂O < 0.1 ppm), and mixed in CH₃NH₂ solution. Powder X-ray diffraction patterns were measured with RIGAKU TTR-III. The lattice parameter of 14.752 Å at room temperature,

which is consistent with a previous report of 14.761 \AA^2 , was determined by Rietveld refinement with the GSAS program¹⁹. The fraction of the fcc polymorphic phase used in this experiment is 70 % (fcc : A15 : bco = 0.70 : 0.23 : 0.07). Here, bco denotes the body-centred-orthorhombic structure^{2,12,20}. This fraction of the fcc phase is comparable to previous reports^{2,12}. The magnetization M was measured using a SQUID magnetometer (Quantum Design MPMS2) in the temperature range of $T > 2 \text{ K}$.

BeCu and NiCrAl/BeCu piston-cylinder-type pressure cells were used to obtain the temperature dependence of magnetization and to perform NMR measurement under pressure, respectively. Daphne oil 7373 is used as a pressure-transmitting medium²¹. The samples are paraffin-embedded to avoid possible degradation by Daphne oil under pressure. The T_c of Sn was monitored to determine pressure at low temperatures.

NMR measurement was carried out using a phase-coherent spectrometer. The usual Hahn-echo method ($\pi/2 - \tau - \pi$), which reduces the A15 contribution to the signal by about a factor of 3, is successfully used to obtain only the fcc phase among its polymorphism^{2,12} [see Fig. 1(a)]. The NMR spectrum is obtained by the Fourier transform of spin echo with a typical pulse sequence of $5\mu\text{s} - \tau - 10\mu\text{s}$ and by plotting the spin echo intensity while sweeping the external magnetic field at a fixed frequency with typical pulse sequence of $60\mu\text{s} - \tau - 120\mu\text{s}$. The nuclear recovery curves for obtaining T_1 were measured using the first pulse length of about $10 \mu\text{s}$.

III. EXPERIMENTAL RESULTS

A. ^{133}Cs -NMR spectrum and T_1

Figure 1(a) shows the ^{133}Cs -NMR spectrum measured at $T = 200 \text{ K}$ and $P = 0$. Crystallographically, fcc Cs_3C_{60} has two ^{133}Cs sites. One is surrounded by octahedral C_{60} balls [Cs_3C_{60} (O)], the other is surrounded by tetrahedral C_{60} balls [Cs_3C_{60} (T)]⁴. Fundamentally, both sites are in a single electronic state, i.e., the temperature dependences of T_1 for both sites are the same¹⁷. On the other hand, it has been known that the other site (T') in fcc A_3C_{60} appears below room temperature^{4,12,18,22-27}. It has been suggested that it comes from some crystal distortions such as displacements or vacancies of A ions, a Jahn-Teller distortion of the C_{60} ion, and a deviation from the expected C_{60} orientation in fcc A_3C_{60} crystals^{22,23,28}. Furthermore, in the $\text{Na}_2\text{AC}_{60}$ compound, which has a simple cubic structure, the merohedral disorder is proposed as the origin of the T' site²⁹. As shown in Fig. 1(a), the sharp peak next to the peak T arises from this T' site [Cs_3C_{60} (T')]. For our Cs_3C_{60} crystal, it is estimated from Fig. 1(a) that the volume fraction ratio of the T site to the T' site is 5.8 : 1 and the volume fraction of the T' site in the entire spectrum is estimated to be 13%, which is consistent with the

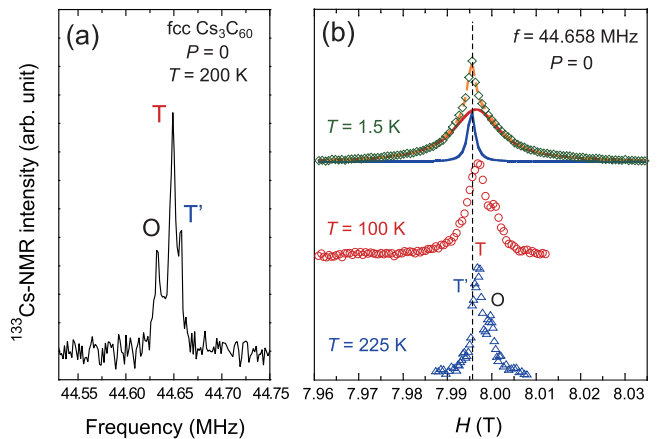


FIG. 1: (a) ^{133}Cs -NMR ($^{133}\gamma = 5.5844 \text{ MHz/T}$) spectrum of fcc Cs_3C_{60} measured at $H = 8.0 \text{ T}$. (b) Temperature dependence of ^{133}Cs -NMR spectrum obtained by sweeping the external magnetic field at the fixed frequency of 44.658 MHz . At $T = 1.5 \text{ K}$, the fitting curves are shown together. The dotted curve is the result of Lorentzian fitting, which consists of broad and sharp peaks. This unambiguously indicates that there exist two fcc Cs_3C_{60} phases with and without internal magnetic field (Mott state and paramagnetic metal). The dotted line indicates the position of the T' peak.

results of previous NMR studies of fcc A_3C_{60} ^{4,12,18,22-28}. Note that the origin of the T' site for fcc A_3C_{60} remains unresolved^{4,12,18,22-28}. However, it has been suggested by double resonance measurement and widely accepted that the T' site forms clusters, which exist randomly in A_3C_{60} crystals without site-to-site correlation.^{22,30}

Figure 1(b) shows the temperature dependence of the ^{133}Cs -NMR spectrum obtained by sweeping the external magnetic field at a fixed frequency of $f = 44.658 \text{ MHz}$. As seen in the figure, the spectrum obtained at $T = 1.5 \text{ K}$ consists of two peaks, a sharp and a broad peak, indicating that there are two electronically different phases with and without an internal magnetic field (Mott and paramagnetic states) as the ground state, as will be discussed later. Notably, as shown by the dotted straight line, the peak position of the sharp peak is consistent with that for the T' site at high temperatures. In addition, the volume fraction ($\sim 15 \%$) of this sharp peak in the entire spectrum at $T = 1.5 \text{ K}$ is also consistent with that for the T' peak at high temperatures. Thus, it is indicated that these broad and sharp peaks originate from the T and T' sites, respectively.

To elucidate the electronic property for fcc Cs_3C_{60} , we measured ^{133}Cs T_1 systematically. For fcc Cs_3C_{60} , since there is no quadrupole interaction at the Cs site owing to highly symmetrical C_{60} balls surrounding Cs ions^{4,12,18}, the nuclear magnetization decay curve for obtaining T_1 for the ^{133}Cs nucleus is a single-exponential function^{4,12,18}, $1 - M(t)/M_0 = \exp(-t/T_1)$, where M_0 and $M(t)$ are the nuclear magnetizations in the thermal

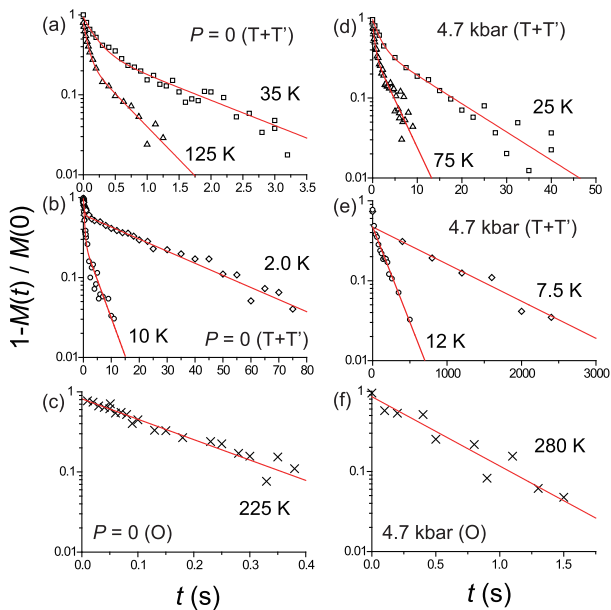


FIG. 2: Typical datasets of nuclear magnetization decay curves for obtaining T_1 for T + T' sites (a), (b) [(d),(e)] and O site (c) [(f)] at $P = 0$ kbar ($P = 4.7$ kbar), respectively. Solid curves are theoretical fitting curves assuming two different T_1 s as parameters as $1 - M(t)/M_0 = \alpha \exp(-t/T_1^T) + (1 - \alpha) \exp(-t/T_1^{T'})$. The contribution of T_1 to the O site to T_1 for T + T' sites is negligible. The T_1 for the O site can be fitted by a single component as $1 - M(t)/M_0 = \alpha \exp(-t/T_1^O)$ (c), (f). Well below T_c ($T = 12$ K and 7.5 K), only the long component T_1 is shown (e).

equilibrium and at a time t after a saturation pulse. Figures 2(a), 2(b), 2(d), and 2(e) show typical datasets of the nuclear magnetization decay curves obtained through the integration of both the T and T' peaks. Figures 2(c) and 2(f) show typical datasets of the nuclear magnetization decay curves obtained through the integration of the O peak. At high temperatures, since the O peak in the spectrum is well separated from the T and T' peaks, we can obtain T_1 for Cs_3C_{60} (O) from a single-component decay curve as $1 - M(t)/M_0 = \alpha \exp(-t/T_1^O)$. The absolute value of T_1^O is consistent with previous reports^{2,12}.

On the other hand, for the T and T' peaks, we observed two T_1 components, i.e., a short one and a long one. The solid curves are fittings consisting of a short T_1 (T_1^S) and a long T_1 (T_1^L) as $1 - M(t)/M_0 = \alpha \exp(-t/T_1^S) + (1 - \alpha) \exp(-t/T_1^L)$. Here, the absolute value of T_1^S is consistent with previously reported T_1 for the T site^{2,12}. However, T_1^L has not been reported for Cs_3C_{60} , although, most probably, it originates from the T' site. As will be discussed later, these two T_1 s show completely different temperature dependences, indicating that the phase separation into two electronic states occurs in our fcc Cs_3C_{60} crystal, which is consistent with the NMR spectrum [see Fig. 1(b)].

The present results are different from the results of pre-

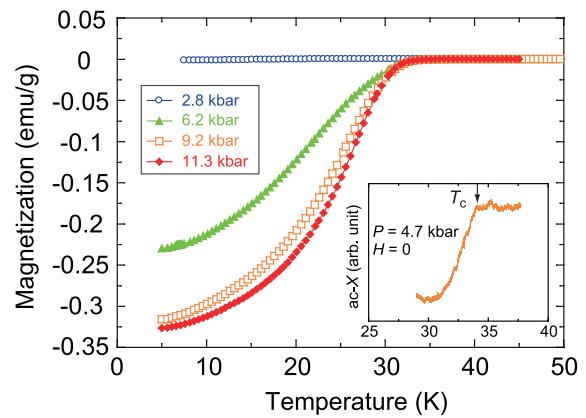


FIG. 3: Temperature and pressure dependences of magnetization for fcc Cs_3C_{60} . The T_c 's (superconducting shielding fractions) of 33.8 K (33.1%), 35.6 K (45.5%), and 34.5 K (47.1%) are obtained at $P = 6.2$, 9.2, and 11.3 kbar, respectively. The inset shows the temperature dependence of the ac susceptibility deduced from the detuning of the NMR tank circuit using an *in situ* NMR coil at $P = 4.7$ kbar under a zero magnetic field. ($T_c = 34.0$ K).

vious NMR studies on Cs_3C_{60} ^{2,12}. One reports a shorter T_1 for the T' site than for the T site, and the temperature dependences of T_1 for both sites are similar². The other report suggested that T_1 's for the T and T' sites are the same³¹. Although the origin of these differences is still unknown, from the temperature dependences of the Cs-NMR spectrum and T_1 , we conclude that our Cs_3C_{60} crystal has different electronic states in the T and T' sites as the ground state. We just speculate that the T' site in our Cs_3C_{60} crystal does not exist as clusters but as domains to form its own phase. A phase separation is often seen in strongly correlated electron systems such as manganese oxides³², and its mechanism might share some similarities across different classes of these materials. Here, we denote these two different phases for the T and T' sites as the Cs_3C_{60} (T) and Cs_3C_{60} (T') phases, respectively. As shown in the recovery curves, this two phases feature does not change under pressure.

B. P -induced superconductivity in fcc Cs_3C_{60}

In this section, we present the results of the pressure-induced superconductivity of the fcc Cs_3C_{60} crystal. Figure 3 shows the temperature dependence of magnetization. As seen in Fig. 3, the superconducting shielding fraction depends on pressure. This is consistent with previous results^{4,12}. From Fig. 3, it is suggested that the superconductivity in full volume is realized only above $P \sim 9$ kbar. This is in contrast with that observed in heavy-fermion compounds³³ or iron-pnictides³⁴ where bulk superconductivity has been observed even in the coexisting state with antiferromagnetism.

C. T and P dependences of $1/T_1T$

Next, we show the evolution of the electronic properties of the Cs_3C_{60} (T) and Cs_3C_{60} (T') phases and its relation to the superconductivity under pressure. Figure 4 shows the temperature dependences of nuclear spin-lattice relaxation rate ($1/T_1$) divided by temperature ($1/T_1T$) for the Cs_3C_{60} (T&O) and Cs_3C_{60} (T') phases measured at $P = 0$ and 4.7 kbar, respectively. In general, $1/T_1T$ is proportional to electron spin susceptibility through the hyperfine coupling constant $A_{\vec{q}}$ as

$$\frac{1}{T_1T} \propto \sum_{\vec{q}} |A_{\vec{q}}|^2 \frac{\chi''(\vec{q}, \omega_0)}{\omega_0}, \quad (1)$$

where ω_0 is the NMR frequency. In fullerides, the dynamic spin susceptibility $\chi''(\vec{q}, \omega)$ is caused by the antiferromagnetic fluctuation with a finite \vec{q} due to the localized electron spins on C_{60} molecules¹⁸. Furthermore, if the lattice parameter decreases, then the overlapping of the C_{60} molecular wave function increases and A_3C_{60} becomes a paramagnetic metal¹⁸. In such a case, since $\chi''(\vec{q}, \omega)$ is proportional to the square of the density of states, $N(E_F)$, at the Fermi level and $A_{\vec{q}}$ is \vec{q} -independent, eq. (1) yields the relation $\frac{1}{T_1T} \propto |A_{\vec{q}}|^2 N(E_F)^2$ (Korringa-law). In particular, in fcc A_3C_{60} crystals, $1/T_1T$'s for the T and O sites are connected through each hyperfine coupling constant¹⁷ as

$$\left(\frac{1}{T_1T}\right)^O \propto \left|\frac{A_{\vec{q}}^O}{A_{\vec{q}}^T}\right|^2 \left(\frac{1}{T_1T}\right)^T. \quad (2)$$

As seen in Fig. 4, $1/T_1T$ for the Cs_3C_{60} (T) phase at $P = 0$ and 4.7 kbar increases with decreasing temperature. This indicates that the antiferromagnetic fluctuation develops as a result of the localization of electron spins on C_{60} balls. At $P = 0$, $1/T_1T$ shows a peak at $T_N \sim 2.5$ K due to antiferromagnetic order. These results at $P = 0$ are consistent with previous μSR measurements². At $P = 4.7$ kbar, we also observed an increase in $1/T_1T$ down to $T = 1.5$ K, suggesting that electron spins are still localized to lead to the Mott state. Notably, no superconducting transition is observed in the Cs_3C_{60} (T) phase at $P = 4.7$ kbar although the onset of pressure-induced superconductivity at $T_c(P) = 34.0$ K is confirmed by ac susceptibility measurement using an *in situ* NMR coil (see Fig. 3 inset). This is one of the most important results of this study, indicating that P_c for the Mott state is above $P > 4.7$ kbar.

On the other hand, we found a very different temperature dependence of $1/T_1T$ for the Cs_3C_{60} (T') phase. At $P = 0$, $1/T_1T$ satisfies the Korringa law at low temperature, indicating that the Cs_3C_{60} (T') phase is a paramagnetic metal. These results are consistent with the Cs-NMR spectrum shown in Fig. 1(b). At $T = 1.5$ K, the Cs-NMR spectrum consists of a broad peak for Cs_3C_{60} (T), which originates from the hyperfine field induced

by the localized electron spins in the Mott state, and a sharp peak for Cs_3C_{60} (T'), where such a field is absent in the metallic state. Thus, it is evidenced that the electronic state for the Cs_3C_{60} (T') phase is completely different from that for the Cs_3C_{60} (T) phase, and that both phases are spatially separated. Since this separation between the Cs_3C_{60} (T') and Cs_3C_{60} (T) phases is realized within the same fcc Cs_3C_{60} crystal, it is suggested that the origin of the T' site for our fcc Cs_3C_{60} crystal is a positive chemical pressure (internal pressure, P_{int}) to delocalize electron spins on C_{60} balls, which causes the metallic state for the Cs_3C_{60} (T') phase.

At $P = 4.7$ kbar, the superconducting transition is observed only in the Cs_3C_{60} (T') phase by a substantial decrease in $1/T_1T$ below $T \sim 30$ K, contrary to the fact that no signature of superconductivity is seen in $1/T_1T$ for the Mott-insulating Cs_3C_{60} (T) phase. This is the source of the pressure-induced superconductivity of Cs_3C_{60} in the low-pressure region. This is consistent with the observation of the partial superconducting shielding fraction at $P < 9$ kbar. From these results, it is clear that the superconductivity for fcc Cs_3C_{60} is induced only for the paramagnetic metal. Notably, the temperature dependence of $1/T_1T$ for the Cs_3C_{60} (T') phase at $P = 4.7$ kbar traces the $1/T_1T$ of ^{133}Cs -NMR for $\text{Rb}_2\text{CsC}_{60}$ (O)¹⁷. Namely, $1/T_1T$ decreases exponentially below T_c and the Korringa law is established above T_c . Since the lattice parameter of fcc $\text{Rb}_2\text{CsC}_{60}$ is smaller than that of fcc Cs_3C_{60} , it is confirmed, from the electronic point of view, that the pressure effect on fcc A_3C_{60} and the variation in its lattice parameter are equivalent.

It has been suggested that the mechanism of superconductivity in $\text{Rb}_2\text{CsC}_{60}$ is a conventional BCS one¹⁷. The present result indicates that the mechanism of Cooper pair formation for fcc Cs_3C_{60} under pressure is also in the framework of the BCS one. In such a case, localized electron spins on C_{60} balls in the Mott state break Cooper pairs³⁵. This also supports the scenario that the origin of the "coexistence" of a Mott insulator and superconductivity in fcc Cs_3C_{60} is the phase separation of the two orders in real space.

IV. DISCUSSION

To explain the present results systematically, we suggest that the phase separation originates from the formation of domains of the Cs_3C_{60} (T') phase due to local P_{int} in fcc Cs_3C_{60} crystals. At $P = 0$, paramagnetic domains of the Cs_3C_{60} (T') phase are formed within the Mott-insulating Cs_3C_{60} (T) phase. At $P = 4.7$ kbar, as shown by the temperature dependence of $1/T_1T$, only domains of the Cs_3C_{60} (T') phase become superconducting and a partial shielding fraction is observed. Note that the superconducting coherence length for fcc Rb_3C_{60} ($T_c = 31$ K) is ~ 19 Å³⁶. From this, it can be speculated that each domain will consist of more than 2 unit cells. Above $P > 4.7$ kbar, an insulator-to-metal transition occurs in

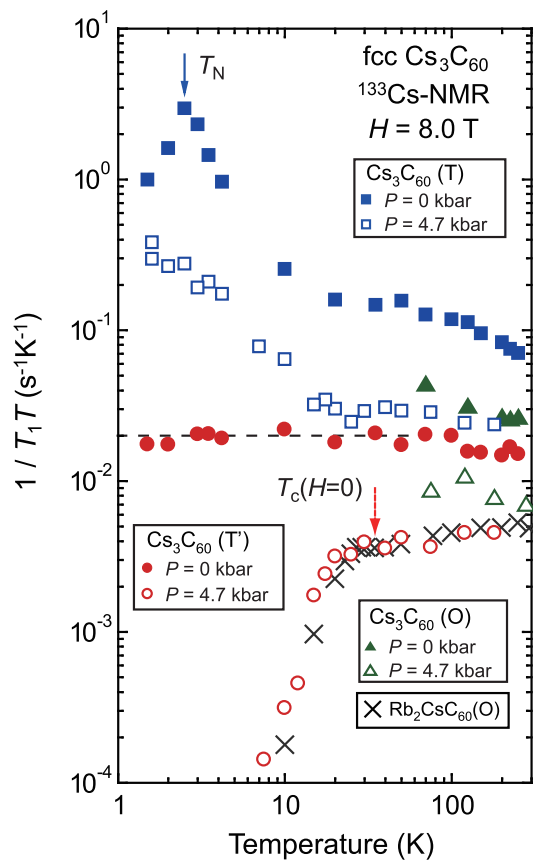


FIG. 4: Temperature and pressure dependences of $^{133}(1/T_1T)$ for fcc Cs_3C_{60} plotted on logarithmic scale. T_1 's for both Cs_3C_{60} (T) and Cs_3C_{60} (T') phases were measured in the range of $1.4 \text{ K} < T < 300 \text{ K}$. The T_1 for Cs_3C_{60} (O) is obtained above $T > 70 \text{ K}$. Solid (open) squares, triangles, and circles indicate $1/T_1T$'s for Cs_3C_{60} (T), Cs_3C_{60} (O), and Cs_3C_{60} (T') at $P = 0$ ($P = 4.7 \text{ kbar}$), respectively. The solid and dotted arrows indicate T_N and $T_c(H=0)$, respectively. $T_c(H=0) = 34.0 \text{ K}$ is determined by ac-susceptibility measurement using an *in situ* NMR coil. The $^{133}(1/T_1T)$ for $\text{Rb}_2\text{CsC}_{60}$ (O) (solid cross) is cited from the literature¹⁷. The dotted line is an eye guide indicating the Korringa law ($1/T_1T = \text{constant}$) at low temperature.

the Cs_3C_{60} (T) phase. Following that, superconducting domain size naturally increases through the proximity effect at the boundary of superconducting domains and the metallic region and thus, the shielding fraction increases. Above $P > 9 \text{ kbar}$, pressure-induced superconductivity also occurs in the Cs_3C_{60} (T) phase and the bulk superconductivity of the fcc Cs_3C_{60} crystal sets in. This scenario can explain the pressure dependence of the superconducting shielding fraction qualitatively and is in good agreement with NMR results as well.

Finally, on the basis of the present results and considering the spatial phase separation due to P_{int} in the fcc Cs_3C_{60} crystal, we present a new phase diagram of fcc Cs_3C_{60} using the unit cell volume (\AA^3) at room temper-

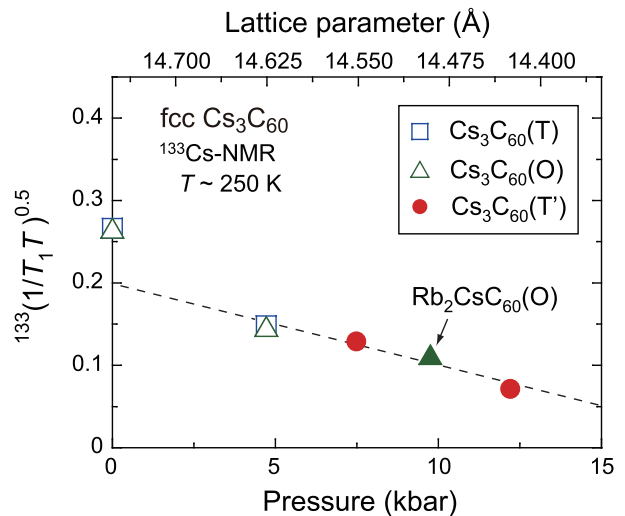


FIG. 5: Open squares indicate the pressure dependence of $^{133}(1/T_1T)^{0.5}$ for Cs_3C_{60} (T). Open (solid) triangles indicate $^{133}(1/T_1T)^{0.5}$ for Cs_3C_{60} (O) [$\text{Rb}_2\text{CsC}_{60}$ (O)]. $1/T_1T$'s for O sites are normalized to that for the T site using the relation $\left(\sqrt{\frac{1}{T_1T}}\right)^O \propto \frac{A^O}{A^T} \left(\sqrt{\frac{1}{T_1T}}\right)^T = \frac{1}{1.63} \left(\sqrt{\frac{1}{T_1T}}\right)^T$. $1/T_1T$ for $\text{Rb}_2\text{CsC}_{60}$ (O) is cited from the literature¹⁷. The normalized $^{133}(1/T_1T)^{0.5}$ for $\text{Rb}_2\text{CsC}_{60}$ (O) corresponds to that for Cs_3C_{60} (T) at $P = 9.7 \text{ kbar}$. Solid circles indicate $^{133}(1/T_1T)^{0.5}$ for Cs_3C_{60} (T') corrected using the internal pressure of $P_{int} = 7.5 \text{ kbar}$. The lattice parameters at room temperature are estimated from the compressibility $\kappa = 0.0053/\text{kbar}$ for fcc Cs_3C_{60} (ref. 4). The lattice parameter of 14.752 \AA is used as the value at $P = 0$ for Cs_3C_{60} (T). The dotted line is an eye guide.

ature. In Fig. 5, we plot the pressure dependences of $^{133}(1/T_1T)^{0.5}$ [$\propto N(E_F)$ for paramagnetic metal] for the T, O, and T' sites of fcc Cs_3C_{60} and for the O site of $\text{Rb}_2\text{CsC}_{60}$ (ref. 17). Here, the previous structural study has revealed that the unit cell volume for fcc Cs_3C_{60} decreases linearly with the compressibility $\kappa = 0.0053/\text{kbar}$ at $P < 10 \text{ kbar}$ ². From this relation, compared with the lattice parameter of 14.752 \AA for our fcc Cs_3C_{60} crystal at $P = 0$, that the lattice parameter of 14.493 \AA for $\text{Rb}_2\text{CsC}_{60}$ (ref. 15) corresponds to the lattice parameter for our fcc Cs_3C_{60} at $P = 9.7 \text{ kbar}$. Meanwhile, using eq. (2), we obtained an exact match in the pressure dependence of $^{133}(1/T_1T)^{0.5}$ for the T and O sites. Notably, offsetting the Cs_3C_{60} (T') data by $P_{int} = 7.5 \text{ kbar}$ will make all data points fall on a straight line above $P > 5 \text{ kbar}$. This evidences that the Mott-insulating Cs_3C_{60} (T) phase becomes metallic above $P > 5 \text{ kbar}$, where $\left(\frac{1}{T_1T}\right)^{0.5} \propto N(E_F) \propto P$ holds. The deviation from a linear relation at $P = 0$ is due to the development of antiferromagnetic fluctuations that lead to the Mott state. From Fig. 5 and using $\kappa = 0.0053/\text{kbar}$, we estimate the lattice parameters of the Cs_3C_{60} (T) and Cs_3C_{60} (T') phases under pressure. The lattice param-

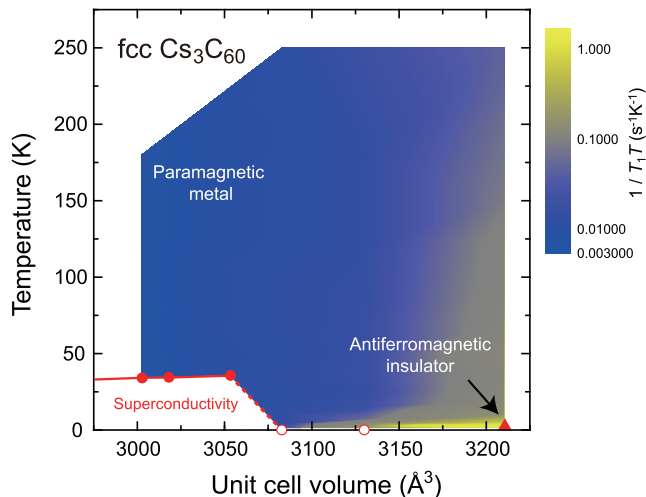


FIG. 6: Unit cell volume vs temperature phase diagram for fcc Cs_3C_{60} plotted using the temperature dependence of $1/T_1T$. Unit cell volume is calculated using the lattice parameter at room temperature. The color coding (bar on right) refers to $1/T_1T$ on the logarithmic scale. The solid circles and triangle indicate T_c and T_N , respectively. The open circles plotted at $T = 1.4$ K indicate that T_c is not found in the measured temperature range ($T > 1.4$ K). The superconducting phase appears with the background of the Korringa law ($1/T_1T = \text{const.}$). Antiferromagnetic fluctuation develops in the region displayed in bright (yellow in color) region.

ter of the Cs_3C_{60} (T) phase at $P = 4.7$ kbar is 14.628 \AA . Since the Cs_3C_{60} (T') phase at $P = 0$ corresponds to the Cs_3C_{60} (T) phase at $P = 7.5$ kbar, the lattice parameter of the Cs_3C_{60} (T') phase at $P = 0$ ($P = 4.7$ kbar) is estimated to be 14.554 \AA (14.426 \AA).

Figure 6 shows a new phase diagram for fcc Cs_3C_{60} . T_N and T_c vs unit cell volume at room temperature are plotted with the magnitude of $1/T_1T$ indicated in brightness. Superconductivity is only seen for the paramagnetic metal [dark (blue in color) region], where the Korringa law ($1/T_1T = \text{const.}$) is well established in the entire temperature range. Antiferromagnetic fluctuations due to the localization of electron spins in C_{60} balls are found in a limited region [bright (yellow in color) region]. The ground states of both antiferromagnetic insulator

(Mott state) and superconductivity are completely separated. This phase diagram is fundamentally different from those of heavy-fermion compounds, high- T_c copper oxides, two-dimensional organic conductors, and ironpnictides. Namely, the superconductivity in fcc Cs_3C_{60} breaks up at the Mott transition. Preventing the localization of electrons on C_{60} balls is rather essential for Cooper pair formation and for finding still higher T_c in this system.

Although the Cs_3C_{60} (T) phase was observed in previous works, we find for the first time that it does not become superconducting at $P = 4.7$ kbar where the partial superconducting transition is observed. Furthermore, the observed phase separation into the Mott state and paramagnetic metal can reasonably explain the unresolved issues in Cs_3C_{60} , the reason (1) why shielding fraction depends on pressure and (2) why antiferromagnetism and superconductivity can "coexist" under pressure.

V. CONCLUSIONS

In this paper, we have presented a ^{133}Cs -NMR study of face-centred cubic structured fulleride Cs_3C_{60} under pressure. Different from previous reports, we find that Cs_3C_{60} crystals show a phase separation between the Mott state and the paramagnetic metal. Our results indicate that the pressure-induced superconductivity in Cs_3C_{60} is realized only for a paramagnetic metal. The phase diagram obtained from the present NMR study strongly indicates that the Mott state and superconductivity are competing orders. The prevention of the localization of electron spins on C_{60} balls is rather essential for finding further higher T_c superconductivity in fullerenes.

Acknowledgments

We thank Takashi Kambe for providing the Cs_3C_{60} samples. S.K. thanks Y. Ihara and K. Ishida for useful discussion. The X-ray diffraction patterns were partly measured in research projects (2007G612) of KEK-PF. This work was supported in part by research grants from MEXT (Nos. 22103004, 22013012, 22740232, and 23102717).

¹ M. Capone *et al.*, Rev. Mod. Phys. **81**, 943 (2009).

² A. Y. Ganin *et al.*, Nat. Mater. **7**, 367 (2008).

³ Y. Takabayashi *et al.*, Science **323**, 1585 (2009).

⁴ A. Y. Ganin *et al.*, Nature **466**, 221 (2010).

⁵ N. D. Mathur *et al.*, Nature **394**, 39 (1998).

⁶ P. A. Lee, N. Nagaosa, and X. G. Wen, Rev. Mod. Phys. **78**, 17 (2006).

⁷ K. Kanoda, J. Phys. Soc. Jpn. **75**, 051007 (2006).

⁸ A. Ardavan *et al.*, J. Phys. Soc. Jpn. **81**, 011004 (2012).

⁹ Y. Kamihara *et al.*, J. Am. Chem. Soc. **130**, 3296 (2008).

¹⁰ T. Oka *et al.*, Phys. Rev. Lett. **108**, 047001 (2012).

¹¹ Y. Iwasa and T. Takenobu, J. Phys. Condens. Matter **15**, R495 (2003).

¹² Y. Ihara *et al.*, Phys. Rev. Lett. **104**, 256402 (2010) and its supplemental material.

¹³ Y. Ihara *et al.*, Europhys. Lett. **94**, 37007 (2011).

¹⁴ A. F. Hebard *et al.*, Nature **350**, 600 (1991).

¹⁵ R. M. Fleming *et al.*, Nature **352**, 787 (1991).

- ¹⁶ K. Tanigaki *et al.*, Nature **352**, 222 (1991).
¹⁷ V. A. Stenger *et al.*, Phys. Rev. Lett. **74**, 1649 (1995).
¹⁸ C. H. Pennington and V. A. Stenger, Rev. Mod. Phys. **68**, 855 (1996).
¹⁹ A. C. Larson and R. B. Von Dreele, Los Alamos National Laboratory Report LAUR, 86-748 (2000).
²⁰ P. Jeglič *et al.*, Phys. Rev. B **80**, 195424 (2009).
²¹ K. Murata *et al.*, Rev. Sci. Instrum. **68**, 2490 (1997).
²² R. E. Walstedt *et al.*, Nature **362**, 611 (1993).
²³ K. Gorny *et al.*, Phys. Rev. Lett. **79**, 5118 (1997).
²⁴ Y. Maniwa *et al.*, Solid State Commun. **82**, 783 (1992).
²⁵ H. Alloul *et al.*, Physica C **235-240**, 2509 (1994).
²⁶ G. Zimmer *et al.*, Phys. Rev. B **53**, 5620 (1996).
²⁷ B. O. Skadtchenko *et al.*, Chem. Mater. **17**, 1467 (2005).
²⁸ M. Apostol *et al.*, Solid. State. Commun. **98**, 253 (1996).
²⁹ P. Matus *et al.*, Phys. Rev. B **74**, 214509 (2006).
³⁰ C. H. Pennington *et al.*, Phys. Rev. B **54**, R6853 (1996).
³¹ Y. Ihara, private communication.
³² E. Dagotto, T. Hotta, and A. Moreo, Phys. Rep. **344**, 1 (2001).
³³ S. Kawasaki *et al.*, Phys. Rev. Lett. **91**, 137001 (2003).
³⁴ Z. Li *et al.*, Phys. Rev. B **86**, 180501(R) (2012).
³⁵ A. Abrikosov and L. P. Gor'kov, Zh. Eksperim. i Teor. Fiz. **39**, 1781 (1960).
³⁶ V. Buntar *et al.*, Phys. Rev. B **72**, 024521 (2005).